DETECTION OF FULL LENGTH MICROTUBULES IN LIVE MICROSCOPY IMAGES

Sylvain Berlemont[1,3], Régis Tournebize[2], Aaron Bensimon[3], Jean-Christophe Olivo-Marin[1]

[1]Quantitative Image Analysis Unit, Institut Pasteur, CNRS URA 2582
[2]Pathogénie Microbienne Moléculaire Unit, Institut Pasteur, INSERM U786
25-28, rue du docteur Roux, 75724 Paris Cedex 15, France
[3]Genomic Vision, Pépinire Paris Santé Cochin, 29, rue du faubourg Saint Jacques, 75014 Paris, France

ABSTRACT

The common way to study microtubule dynamics in microscopy image sequences is to track the growing ends of microtubules. However, this strategy may fail for dense microtubules due to numerous ambiguities in point association. We suggest that detecting and tracking full length microtules, instead of tracking their extremities only, would provide substantial information to resolve these ambiguities. In this paper, we propose a first part toward that end by introducting a fully automated detection method of full length microtubules, with a statistical control of false detections. It is based on the Feature-adapted Beamlet transform which has been successfully used for filament detection [1]. We provide three improvements to our previous work: i) a normalization of beamlet coefficients, ii) a scale-dependent thresholding of beamlets and iii) a novel beamlet chaining algorithm, adapted to microtubules images.

Index Terms— Beamlet transform, Radon transform, steerable filters, feature, microtubule dynamics analysis

1. INTRODUCTION

Microtubules are important components of the cytoskeleton involved in many important cellular functions such as organelles transport, positioning and mitosis [2]. During mitosis, the long and stable network of interphasic microtubules is dramatically remodeled into shorter and more unstable microtubules to build up the mitotic spindle, the structure required for chromosomes segregation. This microtubule reorganisation is due to changes in microtubule properties.

Microtubules are hollow polymers of subunits of alpha-beta tubulin dimers. These thin filaments ($\sim$ 2.5 nm) have the property to grow by addition of subunits at their fastest growing end (the plus end) and shrink by losing tubulin subunits from this end. Although some of the main regulators of microtubule dynamics have been identified and characterized, a detailed view of how microtubule stability is regulated throughout the cell cycle is still lacking.

The authors aknowledge the support of Genomic Vision and A.N.R.T.

The common way to study microtubule dynamics in microscopy image sequence is to track the growing ends of microtubules thanks to a multiple particle tracking algorithm such as presented in [3]. However, this strategy may fail in presence of strong density microtubules due to high level of ambiguities in point association. We suggest that detecting and tracking full length microtules, instead of tracking their extremities only, would provide substantial information to resolve these ambiguities while leading to more precise measurements on microtubule's length, displacement, growing and shrinking rates. Figure 1 shows an example of microtubule growth during interphase.

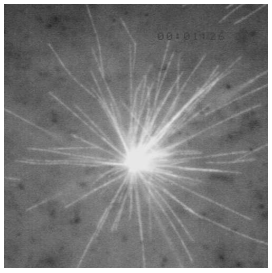

Fig. 1. Full-labeled microtubule growth during interphase.

In this paper, we present the first part of an ongoing project on microtubule dynamics analysis and focus on the detection part. We propose a fully automated detection method of full length microtubules, with a statistical control of false detections. It is based on the Feature-adapted Beamlet transform which has been successfully used in filament detection algorithms [1]. A typical detection process based on such a transform can be described as follows: a) compute the Feature-adapted Beamlet transform of the image, b) normalize beamlet coefficients, c) threshold coefficients, d) put beamlets together (chaining) in order to get a list of detected filaments. These steps are depicted in figure 2. Despite its robustness, that methodology does not provide real statistical control on the detections. To achieve that requirement, we provide three improvements to our previous work: i) a normalization of beamlet coefficients, ii) a scale-dependent

thresholding of beamlets and iii) a novel beamlet chaining algorithm, adapted to microtubules images. In section 2, we recall some key elements of our previous work on Feature-adapted Beamlet transform. Section 3 presents our contributions while section 4 presents some experiments on real data. Finally, section 5 concludes this paper.

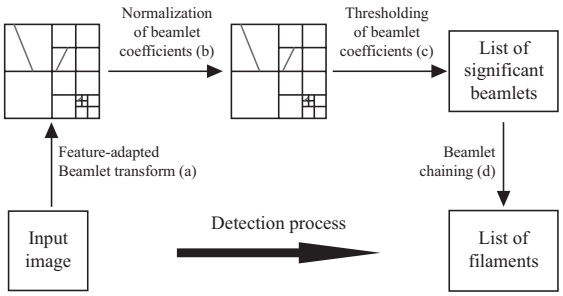

Fig. 2. Workflow of a filament detection process using Feature-adapted Beamlet transform.

2. PREVIOUS WORK

2.1. Beamlet transform

The Beamlet transform introduced in [4] defines a set of dyadically organized line segments (beamlets) occupying a range of dyadic locations and scales, and spanning a full range of orientations. The underlying idea of the Beamlet transform is to compute line integrals only on the set of beamlets, which is an efficient substitute of the entire set of segments for it can approximate any segment and curve by a finite chain of beamlets. The beamlet transform can be computed as follows: 1) define the set of all dyadic squares obtained by recursive partitionning of the image domain and 2) on each square S, compute the classical Radon tranform on the portion of the image induced by S.

2.2. Feature-adapted Radon transform

Recently, a novel Fourier-based approach has been proposed in order to compute the discrete Radon tranform [5]. The method relies on a discrete Fourier slice theorem, which associates the discrete Radon transform with the pseudo-polar Fourier transform. The algorithm is fast since it computes the 2D discrete Radon transform using $O(N \log N)$ operations, where $N = n^2$ is the number of pixels in the image. For a *basically horizontal* line of the form $y = \tan(\theta)x + t$, where the slope $|\tan(\theta)| \leq 1$, the discrete Radon transform associated with such line set is defined as

$$R[I](t,\theta) = \sum_u \tilde{I}(u, \tan(\theta)u + t), \qquad (1)$$

where $\tilde{I}(u,y)$ is an interpolant that takes discrete values in the first argument and continuous values in the second argument. The 1-dimensional interpolation is calculated thanks to a Dirichlet kernel (see [5] for complete details). While this technique provides a quite efficient way to compute discrete Radon transform, it does not take into account any line-profile such as edge or ridge-like profile for the case of filamentary structures. It implies that the Radon and Beamlet transforms are not well-adapted to represent curvilinear objects carrying a specific line-profile. To overcome this limitation, it has been proposed in [6] the Feature-adapted Radon transform. Consider a filter h representing a 2-dimensional line-profile. Let h^θ be a rotated version of h in the direction θ. In a first step, we filter the image I with h^θ before computing equation (1). For a fixed θ, we have

$$R[I * h^\theta](t,\theta) = \sum_u \widetilde{I * h^\theta}(u, \tan(\theta)u + t). \qquad (2)$$

A high coefficient means that the local feature runs significantly along the line $y = \tan(\theta)x + t$. In general, the computation of all these coefficients is not achievable, since it requires to convolve the image and to perform Pseudo-Polar Fourier transform as many times as the number of θ's, *i.e.* $2n$ times. For the special case where h belongs to the class of steerable filters [7], we can write h^θ as a linear combination of basis filters $h^\theta(x,y) = \sum_{j=1}^M k_j(\theta) h^{\theta_j}(x,y)$, where k_j are interpolation functions that only depend on θ and the basis filters h^{θ_j} are independent of θ. A convolution of an image with a steerable filter of arbitrary orientation is then equal to a finite weighted sum of convolutions of the image with each basis filter. It follows that

$$R[I * h^\theta](t,\theta) = \sum_{j=1}^M k_j(\theta) R[I * h^{\theta_j}](t,\theta). \qquad (3)$$

Equation (3) can be evaluated for all parameters (t,θ) in $O(N \log N)$ operations (see [6] for complete details). The extension to the Feature-adapted Beamlet transform is straightforward: instead of using classical Radon transform in the Beamlet transform, the Feature-adapted Radon transform can be applied on all dyadic squares that partition the image domain yielding the Feature-adapted Beamlet transform.

3. STATISTICALLY-CONTROLLED DETECTION OF FILAMENTS

In this section, we propose several improvements to provide a real statistical control regarding the number of false detections. Starting from a simple assumption on image statistics, we first derive the distribution of Feature-adapted Radon coefficients. Then, we propose a novel algorithm that optimizes a cost function in order to select a list of significant segments over the whole set of beamlets. This selection involves a thresholding step that depends on the scale of coefficients. A family of scale-dependent threshold is derived

which garanties a statistical control on the number of false detections. Finally, we propose an adapted beamlet chaining algorithm in order to put beamlets together and provide a list of detected microtubules.

3.1. Normalization of coefficients

Under the assumption that images are corrupted by an additive Gaussian white noise, we derive the following result on the distribution of Feature-adapted Radon coefficients:

Proposition 1. *if $I = (I_i)_{i\in\mathbb{Z}_2}$ are i.i.d. normal variables where $I_i \sim \mathcal{N}(\mu, \sigma^2)$, then we have $R[I * h^\theta](t,\theta) \sim \mathcal{N}(\mu_R, \sigma_R^2)$ where*

$$\mu_R = \mu\|h\|_1 R[\mathbb{1}](t,\theta),$$
$$\sigma_R^2 = \sigma^2\|h\|_2^2 \sum_{u=-n/2}^{n/2-1}\sum_{v=-n/2}^{n/2-1} D_m(\tan(\theta)u + t - v)^2,$$

where $\mathbb{1}(u,v) = 1$ for all (u,v) and D_m is a Dirichlet kernel defined as $D_m(t) = \frac{\sin(\pi t)}{m\sin(\pi t/m)}$ with $m = 2n+1$. It follows that

$$\tilde{R}[I * h^\theta](t,\theta) = \frac{R[I * h^\theta](t,\theta) - \mu_R}{\sigma_R} \sim \mathcal{N}(0,1).$$

The proof is given in [8]. In order to normalize Feature-adapted beamlet coefficients, we proceed as follows: 1) we automatically estimate $\hat{\mu}$ from the median of I and $\hat{\sigma}$ from the median absolute deviation estimation of the Daubechies D8 wavelet coefficients at the 1^{st} scale, 2) for each scale j, $0 \le j \le J$, we compute the maps μ_R and σ_R for every Radon coefficients (t,θ) thanks to proposition 1 and finally, 3) we normalize each coefficient by its associated μ_R and σ_R. Note that if μ and σ are discarded from μ_R and σ_R, these quantities only depend on the filter h and image size and thus, can be precomputed for all scales.

3.2. Selection of beamlets

In this section, we propose a new cost function optimization which selects a list of significant beamlets. A recursive dyadic partition $\mathcal{P}$ of the image domain is any partition, starting from the whole image domain, obtained by recursively choosing between replacing any square of the partition by its decomposition into four dyadic squares or leaving it unsplit. This concept is very similar to the *quadtree* decomposition technique. A beamlet-decorated partition is a partition in which each square is associated with at most one beamlet. We note $\mathcal{P}_j$ the subset of $\mathcal{P}$ of all dyadic squares at scale j. We maximize over all recursive dyadic partition the following cost function:

$$E(\mathcal{P}) = \sum_{j=0}^{J}\sum_{S\in\mathcal{P}_j}\Big(\max_{t,\theta}\Big\{\tilde{R}[I_S * h^\theta](t,\theta)\Big\} - \lambda_j\Big)^+, \quad (4)$$

where I_S is the portion of the image defined by square S and $(\lambda_j)_{0\le j\le J}$ is a family of scale-dependent thresholds. The notation $(x)^+$ stands for x if $x > 0$, 0 otherwise. Note that equation (4) can be solve efficiently by a recursive tree-pruning algorithm due to additivity of the cost function. See [4] for complete details.

3.3. Choice of scale-dependent thresholds

Here we derive the λ_j terms such that they statistically control the number of false detections. We define a simple binary hypothesis test:

$$\begin{cases} H_0\text{: square S is decorated by } \operatorname{argmax}_{t,\theta}\Big\{\tilde{R}[I_S * h^\theta](t,\theta)\Big\} \\ H_1\text{: square S is left undecorated.} \end{cases}$$

For a fixed percentage α of false detection, choosing the null hypothesis while H_1 is true corresponds to

$$P\big[\max_{t,\theta}\Big\{\tilde{R}[I_S * h^\theta](t,\theta)\Big\} \ge \lambda_j\big] = \alpha \quad (5)$$

$$\iff \Big[\int_{-\infty}^{\lambda_j} \frac{1}{\sqrt{2\pi}}\exp^{-\frac{1}{2}x^2}\,dx\Big]^{N_j} = 1-\alpha \quad (6)$$

$$\iff \frac{1}{2^{N_j}}\Big(1 + erf(\frac{\sqrt{2}}{2}\lambda_j)\Big)^{N_j} = 1-\alpha \quad (7)$$

where $N_j = 4n^2$ is the number of Radon coefficients for a dyadic square of size $n = 2^j$. We solve this equation for typical quantiles $\alpha = 1\%, 5\%, 10\%$ in order to exhibit λ_j values for each scale $0 \le j \le J$. Maxima software (http://maxima.sourceforge.net/) has been used to perform these computations.

3.4. Beamlet chaining

We now describe a beamlet chaining algorithm adapted for microtubules images. The objective is to create a list of filaments from a list of beamlets. As shown in figure 1, centrosome, from which microtubules grow and shrink, is located in the center of the image. Then we propose a greedy algorithm that chains one beamlet at once, starting from the centrosome's estimated location to the image boundaries. We convert beamlet coordinates into polar coordinate system and sort them with respect to their radial coordinate in order to traverse the list only once. This algorithm requires $O(N \log N)$ operations to create a list of filaments, where N stands for the number of detected beamlets.

4. EXPERIMENTS

In this section, we experiment our detection method on an image sequence of growing microtubules during interphase. In

order to monitor full length microtubules in live microscopy images, tubulin has been rhodamine-labeled and acquired thanks to an epifluorescence microscope over several time frames.

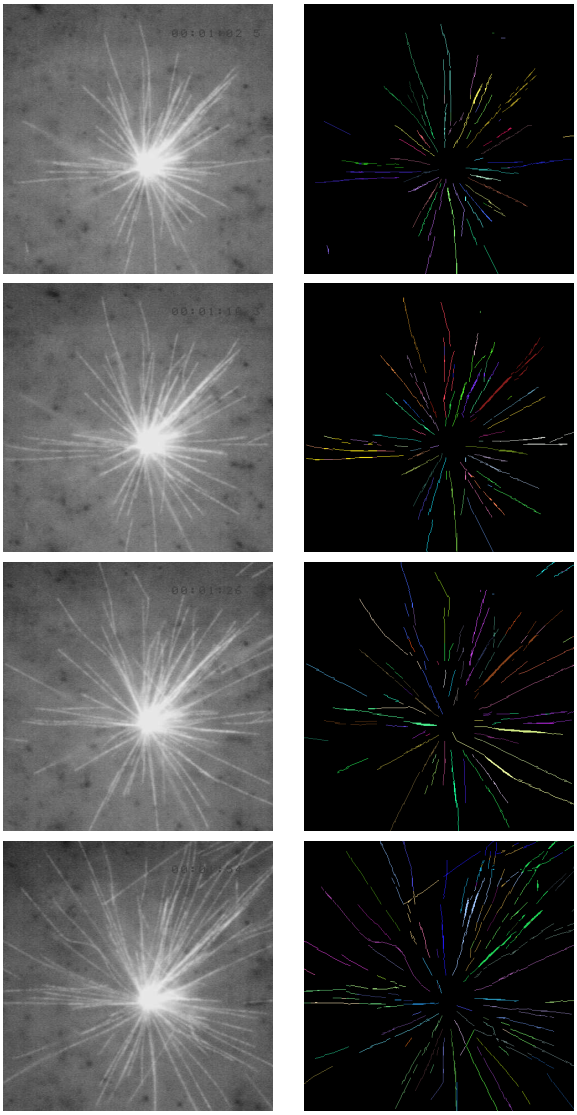

Fig. 3. Detection of full-length microtubules during interphase at t = 24s, 32s, 48s and 76s. Right column shows the detection after chaining step. Each filament is labeled by a single color.

Since microtubules width cannot be resolved by standard microscope, it is acceptable to consider the transverse dimension of such filaments to be small relative to the point spread function width of the microscope. We use a gaussian approximation of the PSF [9] with $\sigma_{PSF} = 0.61 \times \lambda_{em}/N.A. \simeq 0.21\mu m$. For the filter h, we choose a 2^{nd} order filter detector defined in [10] with $\sigma_h = \sigma_{PSF}/\sqrt{2} \simeq 0.14\mu m$. Figure 3 shows the results of detection at different time frames of the sequence. In the second column, each filament is labeled by a single colour. It can be appreciated that microtubules are detected with good accuracy. However, we can notice some errors in the chaining step due to the fact that the assumption that all filaments are growing from the center may not be true. This can be the case when microtubules coming from another centrosome enter into the field.

5. CONCLUSION

In this paper, we have proposed a first part toward quantification of full-length microtubule dynamics in live microscopy images. We have introduced a fully automated detection method of full length microtubules, based on the Feature-adapted Beamlet transform technique, with a statistical control of false detections. To achieve this statistical requirement, we have proposed three improvements to our previous work: $i)$ a normalization of beamlet coefficients, $ii)$ a scale-dependent thresholding of beamlets and $iii)$ a novel beamlet chaining algorithm, adapted to microtubules images. Preliminary results given here are encouraging. The next step now is to embed these detections into a tracking system in order to fully quantify microtubules dynamics.

6. REFERENCES

[1] S. Berlemont, A. Bensimon, and J.-C. Olivo-Marin, "Detection of curvilinear objects in biological noisy image using feature-adapted fast slant stack," in *SPIE conference Wavelets XII, Special Session on Wavelet in Bioimaging*, August 2007.

[2] R. Tournebize, SS. Andersen, F. Verde, M. Dorée, and E. Karsenti AA. Hyman, "Distinct roles of PP1 and PP2A-like phosphatases in control of microtubule dynamics during mitosis," *EMBO Journal*, vol. 16, no. 18, pp. 5537–5549, 1997.

[3] I. Smal, W. Niessen, and E. Meijering, "Advanced particle filtering for multiple object tracking in dynamic fluorescent microscopy images," in *IEEE International Symposium on Biomedical Imaging: From Nano to Macro*, April 2007, pp. 1048–1051.

[4] D. L. Donoho and X. Huo, "Beamlets and multiscale image analysis," in *Multiscale and Multiresolution Methods, Lecture Notes in Computational Science and Engineering*, 2001, vol. 20, pp. 149–196.

[5] A. Averbuch, R.R. Coifman, D.L. Donoho, M. Israeli, Y. Shkolnisky, and I.Sedelnikov, "A framework for discrete integral transformations II - the 2D discrete Radon transforms," *SIAM Journal on Scientific Computing*, 2006, (To appear).

[6] S. Berlemont, A. Bensimon, and J.-C. Olivo-Marin, "Feature-adapted fast slant stack," in *IEEE International Conference on Image Processing*, September 2007, vol. 4, pp. 57–60.

[7] W. T. Freeman and E. H. Adelson, "The design and use of steerable filters," *IEEE Transactions on Pattern Analysis and Machine Intelligence*, vol. 13, no. 9, pp. 891–906, 1991.

[8] S. Berlemont, "Combining linear filtering and multiscale analysis for edge, ridge and curvilinear objects detection," Internal report, Quantitative Image Analysis Unit, Institut Pasteur, CNRS URA 2582, 2008.

[9] B. Zhang, J. Zerubia, and J-C. Olivo-Marin, "Gaussian approximations of fluorescence microscope PSF models," *Journal of Applied Optics*, vol. 46, no. 10, pp. 1819–1829, 2006.

[10] M. Jacob and M. Unser, "Design of steerable filters for feature detection using canny-like criteria," *IEEE Transactions on Pattern Analysis and Machine Intelligence*, vol. 26, no. 8, pp. 1007–1019, August 2004.